Monthly Notices
of the
ROYAL ASTRONOMICAL SOCIETY

MNRAS **493,** 5773–5787 (2020)
Advance Access publication 2020 March 13

doi:10.1093/mnras/staa645

Spectral variability of a sample of extreme variability quasars and implications for the Mg II broad-line region

Qian Yang [1]★ Yue Shen,[1,2] Yu-Ching Chen,[1,2] Xin Liu,[1] James Annis,[3] Santiago Avila [4] Emmanuel Bertin,[5,6] David Brooks,[7] Elizabeth Buckley-Geer,[3] Aurelio Carnero Rosell [8,9] Matias Carrasco Kind [1,2] Jorge Carretero,[10] Luiz da Costa,[8,11] Shantanu Desai,[12] H. Thomas Diehl,[3] Peter Doel,[7] Josh Frieman,[3,13] Juan Garcia-Bellido,[4] Enrique Gaztanaga [14,15] David Gerdes,[16,17] Daniel Gruen [18,19] Robert Gruendl,[1,2] Julia Gschwend,[8,11] Gaston Gutierrez,[3] Devon L. Hollowood,[20] Klaus Honscheid,[21,22] Ben Hoyle [23,24] David James,[25] Elisabeth Krause,[26] Kyler Kuehn,[27] Christopher Lidman [28] Marcos Lima,[8,29] Marcio Maia,[8,11] Jennifer Marshall,[30] Paul Martini,[22,31] Felipe Menanteau,[1,2] Ramon Miquel,[10,32] Andrés Plazas Malagón [33] Eusebio Sanchez,[9] Vic Scarpine,[3] Rafe Schindler,[18] Michael Schubnell,[17] Santiago Serrano,[14,15] Ignacio Sevilla,[9] Mathew Smith [34] Marcelle Soares-Santos [35] Flavia Sobreira,[8,36] Eric Suchyta [37] Molly Swanson,[2] Gregory Tarle,[17] Vinu Vikram[38] and Alistair Walker[39]

Affiliations are listed at the end of the paper

Accepted 2019 October 21. Received 2019 September 12; in original form 2019 April 24

ABSTRACT

We present new Gemini/GMOS optical spectroscopy of 16 extreme variability quasars (EVQs) that dimmed by more than 1.5 mag in the *g* band between the Sloan Digital Sky Survey (SDSS) and the Dark Energy Survey epochs (separated by a few years in the quasar rest frame). These EVQs are selected from quasars in the SDSS Stripe 82 region, covering a redshift range of $0.5 < z < 2.1$. Nearly half of these EVQs brightened significantly (by more than 0.5 mag in the *g* band) in a few years after reaching their previous faintest state, and some EVQs showed rapid (non-blazar) variations of greater than 1–2 mag on time-scales of only months. To increase sample statistics, we use a supplemental sample of 33 EVQs with multi-epoch spectra from SDSS that cover the broad Mg II λ2798 line. Leveraging on the large dynamic range in continuum variability between the multi-epoch spectra, we explore the associated variations in the broad Mg II line, whose variability properties have not been well studied before. The broad Mg II flux varies in the same direction as the continuum flux, albeit with a smaller amplitude, which indicates at least some portion of Mg II is reverberating to continuum changes. However, the full width at half-maximum (FWHM) of Mg II does not vary accordingly as continuum changes for most objects in the sample, in contrast to the case of the broad Balmer lines. Using the width of broad Mg II to estimate the black hole mass with single epoch spectra therefore introduces a luminosity-dependent bias.

Key words: black hole physics – line: profiles – galaxies: active – quasars: general.

1 INTRODUCTION

The canonical unification model of active galactic nucleus (AGN) dictates that Type 2 objects (with only narrow emission lines) are

★ E-mail: qiany@illinois.edu

drawn from the same underlying population as Type 1 objects (with both broad and narrow emission lines), but the AGN continuum and broad-line emission is obscured by a dust 'torus' (Antonucci 1993; Urry & Padovani 1995). However, this static classification scheme is challenged by an increasingly large body of discoveries of quasars that apparently change spectral types on multiyear time-scales(e.g. Denney et al. 2014; LaMassa et al. 2015; MacLeod et al. 2016; McElroy et al. 2016; Ruan et al. 2016; Runnoe et al. 2016; Gezari et al. 2017; Stern et al. 2018; Yang et al. 2018; MacLeod et al. 2019), mostly from recent multi-epoch imaging and spectroscopic surveys of quasars. The broad Balmer emission lines, including Hα, Hβ, and Hγ, and broad helium lines were observed to have dramatically changed between the dim and bright epochs, even completely disappearing or emerging, following large-amplitude variability in the continuum. This population of changing-look quasars (CLQs) challenges the unified model of AGN, and is difficult to understand in the standard accretion disc theory given the observed short time-scale of the changes. They may have profound implications for accretion physics (Lawrence 2018).

The continuum radiation of quasars is observed to vary typically by 0.2 mag on time-scales of months to years (e.g. Vanden Berk et al. 2004; Wilhite et al. 2005; Sesar et al. 2007; Schmidt et al. 2010; MacLeod et al. 2012; Morganson et al. 2014). Rumbaugh et al. (2018) found that approximately 10 per cent of quasars can vary by >1 mag, dubbed extreme variability quasars (EVQs), over an observed baseline of ∼15 yr. Because the broad emission lines are presumably powered by the ionizing continuum, they will reverberate to the continuum variability on the broad-line region (BLR) light-travel time-scales of days to weeks, which is much shorter compared to the BLR dynamical time-scale of the order of a few years. Thus the study of the EVQ population is not only useful to understand accretion physics in the context of extreme variability, but also important to characterize the response of the broad lines to the extreme continuum variability, which in turn will shed light on the kinematics and structure of the BLR.

While there have been numerous variability studies on the broad Hβ line with, e.g. reverberation mapping (RM) data, similar studies on the broad Mg II line have been sparse (e.g. Trevese et al. 2007; Woo 2008; Hryniewicz et al. 2014; Cackett et al. 2015; Sun et al. 2015; Zhu, Sun & Wang 2017). However, the broad Mg II line is an important line, as it is used for RM (Clavel et al. 1991; Reichert et al. 1994; Metzroth, Onken & Peterson 2006; Shen et al. 2016) and single-epoch black hole mass estimation of quasars at redshift $z >$ 1 (e.g. McLure & Jarvis 2002; McLure & Dunlop 2004; Shen et al. 2008, 2011; Wang et al. 2009), and thus it is important to understand the variability properties of broad Mg II as the continuum varies.

Assuming that the BLR is virialized, the BH mass is determined by the BLR size and the virial velocity (e.g. Wandel, Peterson & Malkan 1999). Practically, the width of broad emission line is used as an indicator of the virial velocity assuming that the line is Doppler broadened. For individual object, the inner gas orbits faster in the virial theorem. Under these assumptions, the broad line width should increase (or decrease) as the BLR contracts (or expands) in respond to a decrease (or increase) in the continuum (i.e. the 'breathing' of the BLR). An anticorrelation between the broad-line width and the BLR size (proportional to the continuum luminosity) is expected, and has been seen in broad Hβ (e.g. Park et al. 2012; Shen 2013). However, the situation is much less clear for Mg II and C IV (Shen 2013). The full width at half-maximum (FWHM) of broad Mg II is strongly correlated with that of broad Hβ (e.g. Shen et al. 2008, 2011; Wang et al. 2019), but the range of dispersion seen in the width of Mg II is smaller than that for Hβ for the same objects (Shen et al. 2011), indicating that Mg II is less variable (e.g. Sun et al. 2015) and possibly has slightly different kinematic structure than broad Hβ. In addition, there is a population of galaxy spectra with broad Mg II, but no broad Hβ (e.g. Roig, Blanton & Ross 2014). All these observations suggest that broad Mg II is somewhat different, and a systematic study of Mg II is required to understand its phenomenology and physics.

Motivated by the questions about how EVQs vary and how their broad emission lines vary accordingly, we select a sample of EVQs that vary by more than 1.5 mag in the g band, using data from DES and SDSS. We obtain new Gemini/GMOS optical spectroscopy of 16 EVQs, and compare with earlier SDSS spectra. Our EVQ sample covers a redshift range of $0.5 < z < 2.1$ with Mg II coverage in both SDSS and GMOS spectra for all our targets, providing a unique opportunity to study Mg II variability leveraged on the extreme continuum variability. Compared with previous works on CLQs, most of our targets are at higher redshifts and probe higher quasar luminosities.

In this work we present our new GMOS spectroscopy and study the spectral variability of these 16 EVQs between the SDSS epoch and the more recent GMOS epoch. The paper is organized as follows. Section 2 describes the imaging data from multiple sources and SDSS spectroscopic data. Section 3 outlines the target selection, spectroscopic observations using Gemini/GMOS, and spectral fitting procedures. We present our results in Section 4 and discuss the implications in Section 5. We summarize in Section 6. We use a ΛCDM cosmology with parameters $\Omega_\Lambda = 0.7$, $\Omega_m = 0.3$, and $H_0 = 70$ km s^{-1} Mpc^{-1}.

2 DATA

2.1 Imaging data

The Dark Energy Survey (DES) observed 5000 deg^2 of the sky in five filters ($grizY_{DES}$), using a wide-field camera (DECam) on the 4-m Blanco Telescope (Flaugher et al. 2015). The 10σ single-epoch PSF magnitude limit in the five $grizY$ bands are 23.57, 23.34, 22.78, 22.10, and 20.69, respectively (Abbott et al. 2018). We used 5 yr DES data starting from 2013 (Abbott et al. 2018; Diehl et al. 2018). For the preliminary year five data, we applied the zero-point calibration with an accuracy of ∼0.01–0.02 mag.

SDSS mapped the sky in five filters ($ugriz_{SDSS}$) using a 2.5 m telescope (Gunn et al. 2006) at the Apache Point Observatory (Abazajian et al. 2009), covering 11 663 deg^2 of the sky. SDSS also repeatedly imaged a 120° × 2.5° stripe along the celestial equator centred at zero declination in the Southern Galactic Cap (Stripe 82) from 1998 to 2007. The frequency was increased from 2005 to 2007 for the supernova survey (Frieman et al. 2008). Over the 10 yr duration of the program, there are, on average, more than 60 epochs in the Stripe 82 region.

The Pan-STARRS1 (PS1; Chambers et al. 2016) survey mapped three-quarters of the sky in five broad-band filters ($grizy_{PS1}$), using a 1.8-m telescope with a 1.4 Gigapixel camera. PS1 data were obtained from 2011 to 2014, filling the gap between the SDSS and DES. We used multi-epoch photometry from the detection catalogue in the PS1 Data Release 2 (DR2). For quasars, the magnitude offset between the SDSS and PS1 (DES) g bands is negligible, between −0.053(−0.065) and 0.005(0.008) mag at redshift $z < 2$ (Yang et al. 2018).

PS1 covers the entire SDSS Stripe 82 region, and DES covers most of the Stripe 82 region with R.A. between 21^h and 3^h (approximately 228 square degrees).

2.2 SDSS spectroscopic data

We used the SDSS spectra as the earlier epoch comparison spectra. The SDSS spectroscopy from the SDSS-I/II covers a wavelength range from 3800 to 9200 Å at an average resolution of $R = \lambda/\Delta\lambda \sim 2000$ (Abazajian et al. 2009), ranging from $R \sim 1500$ at 3800 Å to $R \sim 2500$ at 9000 Å.

3 METHODS

3.1 Target selection

3.1.1 Main EVQ sample

Given the large overlap between DES and SDSS within the Stripe 82 region, we carried out a systematic search for EVQs from 9 258 quasars in the Stripe 82 region (MacLeod et al. 2012), with improved calibration (Ivezić et al. 2007; Sesar et al. 2007) and detailed spectral measurements from their SDSS spectra (Shen et al. 2011). Among them, 7 516 were observed by DES, and 95 per cent of them were detected by PS1. Combining the SDSS Stripe 82 and DES light curves, we selected quasars with a maximum g-band variability larger than 1.5 mag over the combined baseline. For the GMOS follow up, we only used DES data up to Y3 (2016) at the time of the proposal. However, in this work we use all the available DES data up to Y5 to construct photometric light curves. In selecting EVQs from the combined SDSS and DES photometric light curves, we rejected points that deviate from the running median of a $\pm$100 d window by more than 0.5 mag, and noisy points with magnitude uncertainties larger than 0.15 mag. This search resulted in 146 quasars. We imposed additional criteria: (1) the quasars were restricted to be those that were in the faint state during the DES epochs; (2) the latest DES epoch (as in Y3 data at the time of the Gemini proposal) is brighter than 22 mag in i-band for reasonably good Gemini spectroscopy; (3) the object did not show frequent large amplitude (>0.5 mag) and rapid (shorter than a month) optical variability, which may be due to blazar activity; (4) it is not a broad absorption line quasar according to the SDSS spectrum, thus excluding objects in which the variability is caused by outflows; (5) we rejected objects with poor or problematic SDSS spectra after visual inspection. We finally selected 27 EVQs, all of which have relatively smooth light curves.

3.1.2 A supplemental sample of EVQs

To increase sample statistics, we add a supplemental sample of EVQs with multi-epoch spectra covering Mg II from the SDSS quasar catalogue[1] in the 14th Data Release (DR14Q; Pâris et al. 2018). The selection criteria are (1) the quality flag 'zWarning' in the quasar catalogue is 0; (2) the median spectral signal-to-noise ratio (S/N) per pixel is higher than 2; (3) the spectrum covers Mg II; (4) the median spectral S/N around Mg II and the continuum at rest-frame 3000 Å, specifically from 2700 to 3100 Å, is higher than 5 to ensure the good quality of our spectral fitting; (5) multi-epoch spectra of the same quasar must all satisfy the criteria from (1) to (4); and (6) for the same quasar, the continuum flux ratio at rest-frame 3000 Å between the brightest and faintest epochs from SDSS is larger than 3, which corresponds to a magnitude difference of 1.2 mag. These criteria result in 33 EVQs at $0.44 < z < 2.33$ selected from SDSS spectroscopy alone, nearly triple our EVQ sample with multi-epoch spectra.

[1] https://data.sdss.org/sas/dr14/eboss/qso/DR14Q/DR14Q_v4_4.fits.

3.2 Spectroscopic observations

We observed 16 of the 27 main-sample EVQs during the Gemini 2018A run from May to September, using the Gemini GMOS-South spectrograph (summarized in Table 1). The targets were observed with the R150 grating and a 0.5 arcsec slit. We choose this configuration to balance the needs for wavelength coverage, spectral resolution, and sensitivity. To mitigate the effect of CCD gaps on coverage, we split the exposures (ExpTime in Table 1) into pairs with central wavelengths of 5800 Å and 6000 Å, respectively. The coadded spectra cover a wavelength range of 4000–10 200 Å with a spectral resolution of $R \sim 630$. The impact of the spectral resolution difference between the GMOS and SDSS spectra is negligible, leading to less than 0.7 per cent difference in line width measurements when FWHM > 4000 km s^{-1} as in the case for the quasars we observed.

The spectra were reduced using standard IRAF[2] routines (Tody 1986, 1993). We used two standard stars (LTT9239 or LTT7987) for our flux calibration. For the 12 objects observed before July 14, the standard stars were observed during the same night of our science observations. For the 4 objects observed on July 14 and September 5, including J2343+0038, J2350+0025, J0140−0035, and J0140+0052, we use the standard star LTT9239 observed on July 12. These four objects, as well as the standard star, were observed on photometric nights.

3.3 Spectral fitting

We fit the spectra using the spectral fitting code from Shen et al. (2018), which models the quasar continuum, broad Fe II emission, and emission line components. The spectra were fit in the rest frame of the quasar after correcting for Galactic reddening using the dust map in Schlegel, Finkbeiner & Davis (1998) and the extinction curve from Cardelli, Clayton & Mathis (1989). The continuum includes a power-law continuum and a positive 3rd-order polynomial accounting for dust reddening internal to the quasar. We used empirical UV Fe II emission templates from the literature (Vestergaard & Wilkes 2001; Tsuzuki et al. 2006; Salviander et al. 2007) covering from 1000 Å to 3500 Å, and an optical Fe II template (3686–7484 Å) from Boroson & Green (1992). We fitted the Fe II emission with three free parameters: normalization, broadening, and wavelength shift. We first fit the continuum and Fe II emission together, choosing a few continuum windows. For instance, to avoid the influence of Mg II emission, we masked the region between 2675 Å and 2925 Å. Then, we subtracted the continuum and Fe II emission components, and fitted the other emission lines. Following Shen et al. (2018), we used three (one) Gaussian components for the broad (narrow) Hβ line, and two Gaussian components for broad Mg II. In addition, we used two Gaussian components for the narrow Mg II $\lambda\lambda$2796, 2803 Å doublet (Wang et al. 2009). To quantify the measurement uncertainties, we used a Monte Carlo approach by adding a random Gaussian deviate to the flux at each pixel, with the Gaussian σ equal to the spectral error at that pixel. We measured the continuum or line properties and their uncertainties using the median value and the semi-amplitude of the range enclosing the 16th and 84th percentiles of the distribution from 50 trials. Our fitting results show that the narrow emission line luminosity is consistent between the SDSS

[2] IRAF is the Image Reduction and Analysis Facility, written and supported by the National Optical Astronomy Observatories (NOAO) operated by the Association of Universities for Research in Astronomy (AURA) under cooperative agreement with the National Science Foundation.

Table 1. Variability of EVQs.

Name	R.A.	Dec.	Redshift	SDSS	Gemini 2018	ExpTime (s)	$\Delta g_{\rm max}$ (mag)	$\Delta g_{\rm phot}$ (mag)	$\Delta g_{\rm spec}$ (mag)	$\Delta g_{\rm back}$ (mag)
J2159+0005	21:59:44.32	+00:05:27.8	0.936	2001-09-21	05-12	675 × 4	2.590 ± 0.068	2.207 ± 0.058	2.442 ± 0.041	−0.050 ± 0.088
J0140+0052	01:40:27.89	+00:52:12.5	1.020	2004-11-06	09-05	675 × 4	2.272 ± 0.067	1.647 ± 0.061	0.312 ± 0.013	−0.078 ± 0.086
J2213−0037	22:13:12.08	−00:37:25.6	2.063	2003-09-30	07-10	675 × 4	2.258 ± 0.096	1.585 ± 0.086	1.148 ± 0.063	−0.176 ± 0.123
J2252+0004	22:52:50.73	+00:04:18.3	1.001	2001-09-26	07-10	675 × 4	2.137 ± 0.042	1.517 ± 0.050	0.708 ± 0.021	−0.121 ± 0.062
J2217+0029	22:17:39.23	+00:29:04.4	1.643	2003-08-22	06-17	450 × 2	1.953 ± 0.038	1.388 ± 0.037	0.974 ± 0.027	−0.297 ± 0.048
J2249+0047	22:49:24.01	+00:47:50.4	1.360	2001-09-26	06-17	675 × 4	2.419 ± 0.090	1.249 ± 0.072	1.202 ± 0.043	−0.344 ± 0.110
J2228−0032	22:28:36.23	−00:32:02.9	1.032	2001-08-22	07-10	900 × 2	1.800 ± 0.033	1.188 ± 0.029	0.871 ± 0.039	−0.216 ± 0.039
J2343+0038	23:43:07.38	+00:38:54.7	0.667	2002-09-08	07-14	450 × 1	1.841 ± 0.042	1.104 ± 0.047	0.840 ± 0.037	0.000 ± 0.056
J2328−0053	23:28:38.04	−00:53:13.6	1.551	2001-10-17	07-10	675 × 4	1.971 ± 0.048	1.020 ± 0.034	0.623 ± 0.019	−0.859 ± 0.054
J2338−0101	23:38:53.44	−01:01:19.4	1.483	2002-09-08	07-12	900 × 2	2.024 ± 0.056	0.949 ± 0.052	0.635 ± 0.025	−0.682 ± 0.069
J2335−0049	23:35:17.82	−00:49:27.0	0.671	2001-10-17	07-12	450 × 2	1.753 ± 0.082	0.949 ± 0.032	0.459 ± 0.096	−0.319 ± 0.081
J0140−0035	01:40:48.62	−00:35:00.9	1.383	2003-01-05	09-05	675 × 4	2.255 ± 0.068	0.863 ± 0.045	0.115 ± 0.014	−1.067 ± 0.076
J2141−0016	21:41:30.61	−00:16:49.1	1.282	2004-08-10	05-12	675 × 4	1.768 ± 0.039	0.622 ± 0.083	1.074 ± 0.025	−1.035 ± 0.088
J0048−0113	00:48:26.09	−01:13:10.7	1.034	2003-09-01	07-09	675 × 4	1.695 ± 0.052	0.479 ± 0.040	0.453 ± 0.018	−0.836 ± 0.052
J2209−0055	22:09:08.24	−00:55:58.8	0.528	2000-09-01	05-12	450 × 2	1.966 ± 0.075	0.251 ± 0.017	1.065 ± 0.007	−1.715 ± 0.076
J2350+0025	23:50:40.09	+00:25:58.9	1.062	2002-09-06	07-14	900 × 2	2.101 ± 0.078	0.141 ± 0.018	−0.217 ± 0.005	−1.890 ± 0.078

The table is ranked by $\Delta g_{\rm phot}$, which is the g-band magnitude difference between imaging photometry closest to the Gemini and SDSS spectra epochs. $\Delta g_{\rm max}$ is the maximum variability in the g band. $\Delta g_{\rm spec}$ is the spectrophotometry magnitude difference with the SDSS and Gemini spectra convolved with the SDSS g-band filter. $\Delta g_{\rm back}$ is the g-band magnitude difference between the latest DES imaging epoch and the faintest DES epoch.

and GMOS spectra, as the narrow-line flux is expected to remain constant on multiyear time-scales for our quasars. For example, the narrow [O II] λ3728 luminosity for J2159+0005 is $10^{42.34\pm0.05}$ and $10^{42.30\pm0.01}$ erg s^{-1} from the SDSS and GMOS spectra, indicating that our flux calibration is reasonably accurate.

4 RESULTS

We summarize the photometric variability of the main-sample EVQs observed by Gemini in Table 1. $\Delta g_{\rm max}$ is the maximum variability in the g band from the SDSS, PS1, and DES observations. All of them have $\Delta g_{\rm max}$ larger than 1.5 mag. $\Delta g_{\rm phot}$ is the g-band magnitude difference between imaging photometry closest to the Gemini and SDSS spectra epochs. The majority of them re-brightened since they were initially selected in the first 3 yr of DES (see their light curves in the left-hand panels of Figs 1 and A1). There are only four with $\Delta g_{\rm phot} > 1.5$ mag, and nine with $\Delta g_{\rm phot} > 1.0$ mag. $\Delta g_{\rm spec}$ is the magnitude difference between the Gemini and SDSS spectra convolved with the SDSS g-band filter curve. $\Delta g_{\rm back}$ is the g-band magnitude difference between the latest DES imaging epoch and the faintest epoch in earlier DES data, describing how much they have brightened since. Among them, nine EVQs did not vary much with $-0.3 \leq \Delta g_{\rm back} \leq 0$, and seven EVQs brightened with $-1.7 < \Delta g_{\rm back} < -0.6$. Hence nearly half of them have significantly brightened (by more than 0.5 mag) since the faintest epoch, which is consistent with the findings in MacLeod et al. (2019). The light curves show that the extreme variability mostly occurs over a few years, but can also occur on much shorter time-scale. For example, J0140+0052 brightened by ∼2 mag from the GMOS spectral epoch to the last DES epoch (less than 1 yr in the observed frame), and J2209−0055 brightened by ∼1 mag and then again dimmed by ∼1 mag from 2016 to 2018. This is consistent with the type transition time-scale of CLQs spanning from 0.9 to 13 yr in Yang et al. (2018).

J2159+0005 is an EVQ that has been dimming continuously since 2001 as seen from its light curves in the g and r bands (shown in Fig. 1). The latest DES photometry of J2159+0005 is >2 mag fainter than the earlier SDSS photometry in 2001. The right-hand panel in Fig. 1 shows that its continuum became much fainter and redder. Fig. 2 shows our fitting results around Mg II and Hβ. While there is no detectable broad Hβ flux in the GMOS spectrum, broad Mg II is still visible (albeit at reduced flux; see below). The narrow Mg II emission on top of the broad-line emission is more distinctive in the faint state spectrum. We witness a normal blue quasar changing to a quasar with a broad Mg II emission line but no broad Hβ emission line, which bears some similarities to the objects presented in Roig et al. (2014), and similar to those CLQs presented in MacLeod et al. (2019). Although the SDSS spectrum does not cover Hβ, this quasar is possibly a CLQ with the highest redshift of $z = 0.936$ known to date. It is plausible that some broad-line quasars at redshift $z > 1$, where Hβ moves out of the optical window, with a red continuum are similar to J2159+0005 seen at redshift $z < 1$.

EVQ J2343+0038 is a CLQ at $z = 0.667$, based on the behaviour of Hβ. It has broad Hβ emission with $L_{H\beta} = 10^{42.32\pm0.09}$ erg s^{-1} and $\rm FWHM_{H\beta} = 4068 \pm 1980$ km s^{-1} in the bright state from the SDSS spectrum. In the dim state, in the GMOS spectrum, the broad Hβ emission has disappeared and we can clearly see Hβ in absorption instead.

The light curves and spectra of the other 14 EVQs are listed in the Appendix. Hβ is available in eight GMOS spectra, in four of them Hβ is broad in the faint state (J0140+0052, J0048−0113, J2209−0055, and J2350+0025), in one it is narrow (J2159+0005), in one it is absorption (J2343+0038), and in other two Hβ is absent (J2252+0004 and J2228−0032). The Hβ and [O III] lines in J2252+0004 and J2228−0032 are marginally present probably because these lines lie beyond 10 000 Å, where the S/N is too low to verify the existence of these lines. Hβ is only available in three of the SDSS spectra, including J2343+0038, J2335−0049, and J2209−0055. Unfortunately, Hβ of J2335−0049 lands within a CCD gap, and we accidentally failed to obtain one exposure for it with the central wavelength at 6000 Å. The Hβ emission of J2209−0055 is broad in both epochs, and its light curves show that it brightened before its GMOS spectrum was taken. The continuum of J2141−0016, at $\lambda < 2200$ Å in the rest frame, becomes much redder when it fades, similar to cases in Guo & Gu (2016), Ross et al. (2018). But the S/N of the GMOS spectra near 4000 Å is low, and a higher quality spectrum is needed to confirm this result.

Broad Mg II line remains visible in all 16 EVQs in both bright and faint epochs. We fit the SDSS and GMOS spectra in detail to analyse their continuum and emission-line properties, and explore Mg II variability in Sections 4.1 and 4.2.

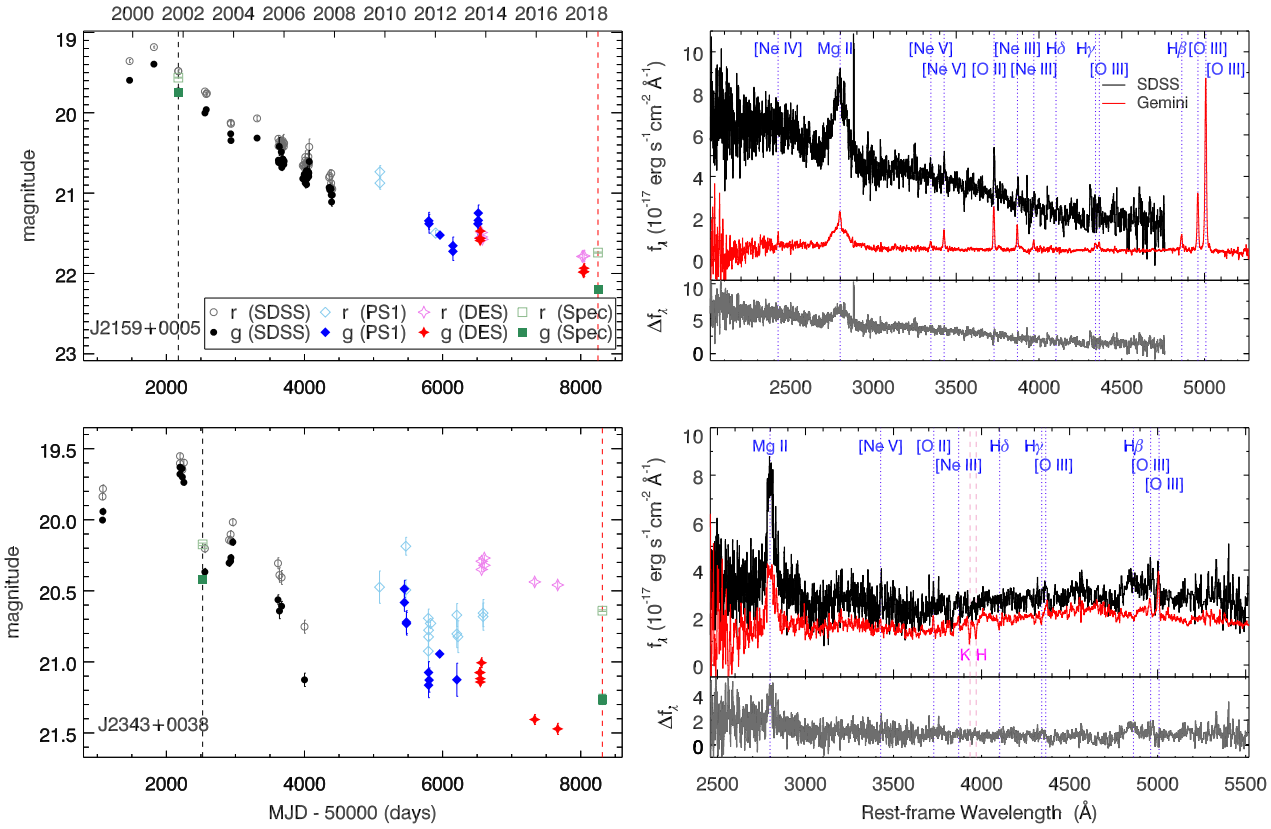

Figure 1. Two EVQs that have changed their spectroscopic appearance, J2159+0005 (upper panels) and J2343+0038 (bottom panels). Left: the light curves in the *g* (filled markers) and *r* (open markers) bands. The photometric data are from the SDSS *g*/*r* (black/grey circles), PS1 *g*/*r* (blue/light-blue diamonds), and DES *g*/*r* (red/violet stars) bands. The vertical dashed lines mark the epochs of the SDSS (black) and recent GMOS (red) spectra. The spectrophotometric magnitude is computed from convolving the spectrum with SDSS *g*-and *r*-band filter curves (green/light-green squares). Right: the spectrum at the earlier epoch (SDSS, black) and the most recent epoch (GMOS, red). The spectra were smoothed with a 3-pixel boxcar. The bottom panel shows the difference, Δf_λ, between the bright and faint epochs. The upper-left panel shows that J2159+0005 faded consistently continuously since ∼2001. In the dim state, there is no detectable broad Hβ emission line, but broad Mg II is still visible. Although the SDSS spectrum does not cover Hβ, this quasar is possibly a CLQ. If confirmed, it would be the most distant one known to date at $z = 0.936$. J2343+0038 is a CLQ as the broad Hβ emission, that is visible in the SDSS spectrum, disappears when the quasar is fainter.

4.1 Mg II line variation

Our EVQ sample reveals that the broad Mg II line does vary in the same direction as the continuum. We summarize the spectral fitting of the main-sample EVQs in Table 2. Fig. 3 shows the variability of broad Mg II line luminosity between the two spectroscopic epochs, $\Delta\log L$(Mg II), as a function of the 3000 Å continuum luminosity variability between the same two epochs, $\Delta\log L$(3000 Å) (in the left-hand panel). The filled black dots are the 16 main-sample EVQs selected from SDSS and DES and followed up with Gemini, and the open grey circles represent the additional EVQs selected from SDSS. The broad Mg II line luminosity increases when the continuum luminosity increases, as naively expected from photoionization. We perform least-square fits to the main EVQ sample of 16 objects, forcing the line to cross [0,0]. We obtain

$$\Delta\log L(\mathrm{Mg\,II}) = (0.39 \pm 0.07) \times \Delta\log L(3000\,\text{Å}). \quad (1)$$

The result for the combined sample, including the main sample and the supplemental sample, is

$$\Delta\log L(\mathrm{Mg\,II}) = (0.47 \pm 0.05) \times \Delta\log L(3000\,\text{Å}). \quad (2)$$

The variation of broad Mg II is indeed smaller than that in the continuum, but still echoes the continuum variation to some extent. This result suggests that at least some part of broad Mg II reverberates to continuum changes, or that the continuum flux that ionizes broad Mg II varies less than the continuum at rest-frame 3000 Å. It is interesting to note that Bruce et al. (2017) found that Mg II flux does not seem to respond to continuum variations in two extreme variability quasars, where the extreme variability can be caused by rare, high-amplitude microlensing events.

The weaker Mg II variations relative to the nearby continuum variations also manifests as an anticorrelation between the equivalent width (W_λ hereafter) of Mg II, $\log W_\lambda$(Mg II), with continuum luminosity, $\log L$(3000 Å), which is the well-known Baldwin effect (e.g. Baldwin 1977; Green, Forster & Kuraszkiewicz 2001). In the right-had panel of Fig. 3, we fit linear regressions and obtain

$$\log W_\lambda(\mathrm{Mg\,II}) = (-0.47 \pm 0.07) \times \log L(3000\,\text{Å}) + (23.01 \pm 2.97), \quad (3)$$

for the main sample, and

$$\log W_\lambda(\mathrm{Mg\,II}) = (-0.33 \pm 0.03) \times \log L(3000\,\text{Å}) + (16.91 \pm 1.31), \quad (4)$$

for the combined sample. For the same object, the W_λ increases when the continuum becomes fainter (listed in Table 2). For the most variable EVQ, J2159+0005, in this sample, the $\log W_\lambda$(Mg II)

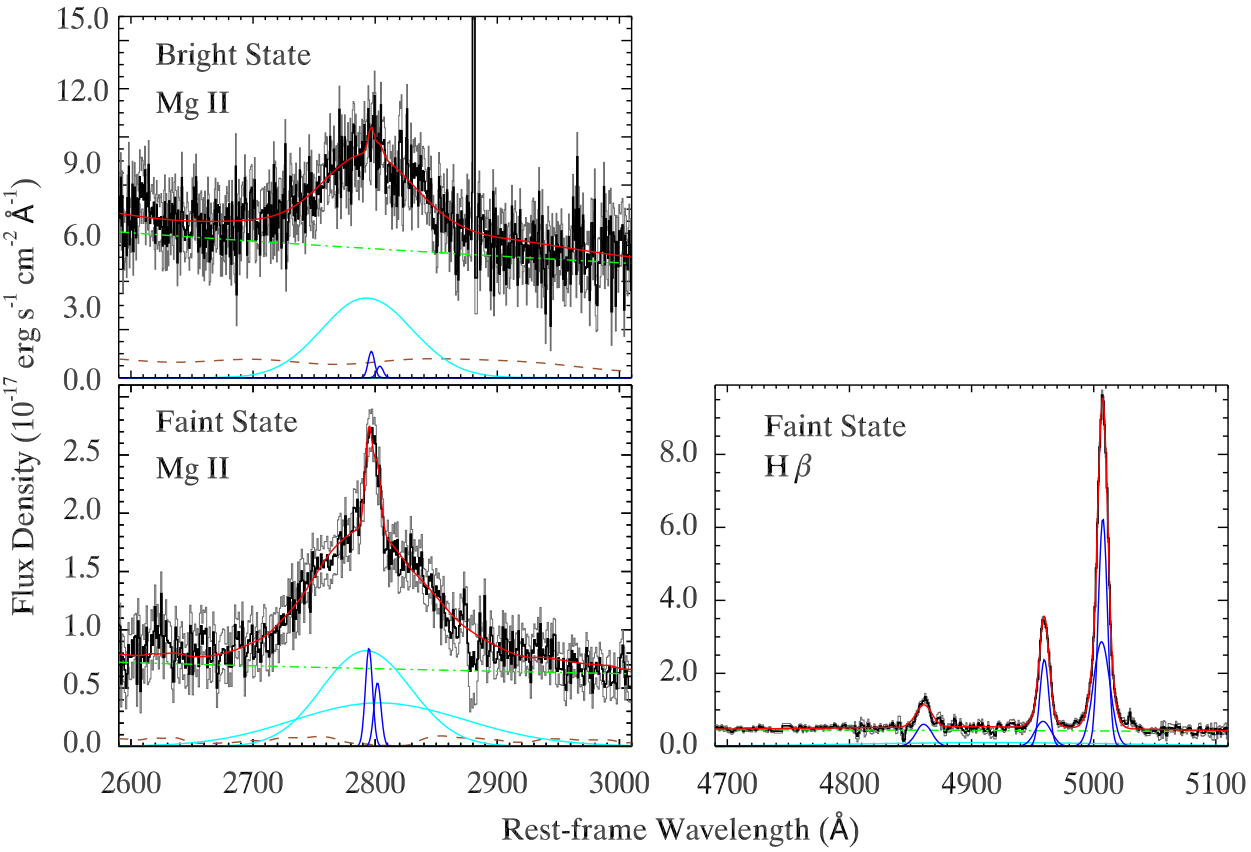

Figure 2. Spectral fitting of EVQ J2159+0005. In the two left-hand panels, the region around Mg II is shown for the spectra obtained with SDSS (upper) and Gemini (lower). The right-hand panel centres on Hβ and [O III]$\lambda\lambda$4959, 5007Å. The black histogram is the spectrum; the red line is the sum of continuum (green dot–dashed line), broad (cyan), and narrow (blue) emission lines, and Fe II emission (brown dashed line). When the continuum faded, there is no broad Hβ detected above 1σ, meanwhile the broad Mg II emission is still apparent. The narrow Mg II emission is visible on top of the broad component.

increases from $10^{1.76\pm0.03}$ to $10^{2.33\pm0.02}$ Å when the continuum L(3000 Å) dims from $10^{45.9\pm0.01}$ to $10^{44.21\pm0.01}$ erg s^{-1}. The variable W_λ indicates that the dramatic decrease in continuum and Mg II is not caused by variable dust reddening.

4.2 Mg II line width

In contrast to the flux, we found that the velocity width (in terms of FWHM) of the broad Mg II line barely changes with luminosity for the bulk of the sample. For J2159+0005, which has the most dramatic change in continuum flux, the broad Mg II component has a FWHM of 9881 ± 693 km s^{-1} for the bright state and a FWHM of 10858 ± 579 km s^{-1} for the faint state, resulting in a change of FWHM of 977 ± 903 km s^{-1}. Assuming that the gas clouds emitting broad Mg II are virialized, the BH mass is

$$M_{\rm BH} = \frac{V^2 R}{G} = f\frac{W^2 R}{G}, \quad (5)$$

where V is the virial velocity, R is the BLR radius, f is a scalefactor that accounts for the orientation, kinematics, and structure of the BLR, and W is the width of the broad line assuming that the broad line is Doppler broadened by virial motion. If the BLR size increases as continuum luminosity increases, as observed for broad Hβ as $R \propto L^{0.5}$ as found in local RM studies or based on the simple photoionization argument, then a relation between the EW and luminosity of the form $\Delta\log W = -0.25\Delta\log L$ is expected. Fig. 4 shows the changes of broad Mg II FWHM between the bright and faint epochs, Δlog FWHM (Mg II), as a function of $\Delta\log L$(3000 Å), the corresponding changes of the continuum luminosity. Our results show that the broad Mg II width does not vary as expected from the simple virial relation above, in sharp contrast to the behaviour of broad Hβ (e.g. Park et al. 2012; Shen 2013). Fitting a linear regression model to our main EVQ sample, we obtain

$$\Delta\log\,\mathrm{FWHM\,(Mg\,II)} = (-0.013 \pm 0.030)\Delta\log L(3000\,\text{Å}). \quad (6)$$

For the combined EVQ sample we obtain

$$\Delta\log\,\mathrm{FWHM\,(Mg\,II)} = (0.012 \pm 0.012)\Delta\log L(3000\,\text{Å}). \quad (7)$$

In both cases the broad Mg II FWHM remains more or less constant despite the large changes in the continuum luminosity, which is consistent with the findings in Shen (2013).

To eliminate a possibility that variable fitting of Fe II emission compromises the line width variation of Mg II, we do a test by fixing the Fe II parameters for the two epochs of the same object. We get

$$\Delta\log\,\mathrm{FWHM\,(Mg\,II)} = (-0.016 \pm 0.030)\Delta\log L(3000\,\text{Å}), \quad (8)$$

for the main EVQ sample, and

$$\Delta\log\,\mathrm{FWHM\,(Mg\,II)} = (0.019 \pm 0.012)\Delta\log L(3000\,\text{Å}), \quad (9)$$

for the combined sample. The result shows that the line width of Mg II barely changes, irrespective of our approach.

We discuss the potential causes of the non-variable broad Mg II FWHM and its implications for virial BH mass estimation using Mg II in Section 5.

Table 2. Spectral Fitting to the Two-Epoch Spectra.

Name	MJD (days)	logL(3000 Å) (erg s^{-1})	logL(Mg II) (erg s^{-1})	FWHM(Mg II) (km s^{-1})	logW_λ(Mg II) (Å)	M_{BH} (10^8 $M_\odot$)
J2159+0005	52 173	45.09 ± 0.01	43.43 ± 0.02	9847 ± 590	1.76 ± 0.03	14.76 ± 1.74
	58 250	44.21 ± 0.01	43.09 ± 0.02	10826 ± 1334	2.33 ± 0.02	5.03 ± 1.18
J0140+0052	53 315	45.12 ± 0.01	43.18 ± 0.03	4384 ± 914	1.49 ± 0.03	3.05 ± 1.25
	58 366	44.90 ± 0.00	43.35 ± 0.02	6104 ± 245	1.88 ± 0.02	4.33 ± 0.35
J2213−0037	52 912	45.61 ± 0.04	43.91 ± 0.11	9633 ± 5678	1.77 ± 0.12	29.74 ± 31.98
	58 309	44.99 ± 0.02	43.55 ± 0.02	7630 ± 671	1.96 ± 0.03	7.63 ± 1.30
J2252+0004	52 178	45.24 ± 0.01	43.37 ± 0.03	7918 ± 1256	1.55 ± 0.03	11.85 ± 3.76
	58 309	44.80 ± 0.00	43.25 ± 0.01	7979 ± 506	1.86 ± 0.01	6.38 ± 0.77
J2217+0029	52 873	45.63 ± 0.01	43.86 ± 0.05	6500 ± 983	1.69 ± 0.05	13.92 ± 4.08
	58 286	45.25 ± 0.00	43.55 ± 0.04	6431 ± 710	1.71 ± 0.03	7.90 ± 1.77
J2249+0047	52 178	45.09 ± 0.01	43.45 ± 0.04	12230 ± 992	1.79 ± 0.04	22.73 ± 3.59
	58 286	44.72 ± 0.00	43.39 ± 0.01	10863 ± 362	2.09 ± 0.01	10.51 ± 0.68
J2228−0032	52 143	45.36 ± 0.00	43.69 ± 0.02	13727 ± 943	1.76 ± 0.02	42.08 ± 5.60
	58 309	44.90 ± 0.01	43.59 ± 0.01	14021 ± 775	2.11 ± 0.01	22.81 ± 2.74
J2343+0038	52 525	44.38 ± 0.01	43.13 ± 0.08	4907 ± 433	2.20 ± 0.07	1.32 ± 0.21
	58 313	44.13 ± 0.01	42.72 ± 0.03	6009 ± 666	2.06 ± 0.05	1.40 ± 0.31
J2328−0053	52 199	45.35 ± 0.02	43.74 ± 0.04	7468 ± 829	1.79 ± 0.05	12.28 ± 2.68
	58 309	45.01 ± 0.00	43.56 ± 0.01	6230 ± 466	1.97 ± 0.01	5.28 ± 0.82
J2338−0101	52 525	45.38 ± 0.01	43.51 ± 0.04	5090 ± 1117	1.56 ± 0.05	5.96 ± 2.49
	58 311	45.19 ± 0.00	43.49 ± 0.03	6781 ± 929	1.73 ± 0.03	8.05 ± 2.09
J2335−0049	52 199	44.53 ± 0.01	43.18 ± 0.05	6360 ± 919	2.10 ± 0.07	2.76 ± 0.81
	58 311	44.39 ± 0.02	42.85 ± 0.05	5079 ± 715	1.87 ± 0.05	1.43 ± 0.40
J0140−0035	52 644	45.22 ± 0.01	43.51 ± 0.03	4004 ± 935	1.71 ± 0.04	2.91 ± 1.44
	58 366	45.12 ± 0.00	43.55 ± 0.04	4978 ± 1034	1.85 ± 0.04	3.94 ± 1.46
J2141−0016	53 227	45.19 ± 0.01	43.62 ± 0.03	4844 ± 439	1.86 ± 0.03	4.08 ± 0.73
	58 250	45.02 ± 0.00	43.36 ± 0.01	4643 ± 267	1.76 ± 0.01	2.98 ± 0.36
J0048−0113	52 883	44.86 ± 0.01	43.26 ± 0.07	5000 ± 821	1.83 ± 0.08	2.75 ± 0.87
	58 308	44.74 ± 0.00	43.18 ± 0.02	4671 ± 516	1.89 ± 0.02	2.01 ± 0.45
J2209−0055	51 788	45.02 ± 0.00	43.37 ± 0.02	6184 ± 393	1.78 ± 0.02	5.24 ± 0.68
	58 250	44.53 ± 0.01	43.00 ± 0.03	5643 ± 787	1.89 ± 0.03	2.16 ± 0.64
J2350+0025	52 523	45.31 ± 0.01	43.62 ± 0.02	4968 ± 478	1.73 ± 0.02	5.11 ± 0.98
	58 313	45.38 ± 0.00	43.69 ± 0.01	4521 ± 138	1.72 ± 0.01	4.71 ± 0.29

M_{BH} is the black hole mass estimated based on the single-epoch recipe based on Mg II in McLure & Dunlop (2004). This table is ranked in the same order as Table 1, from the most dimmed to the least dimmed quasars.

5 DISCUSSION

The coordinated variations in the continuum flux and in the broad Mg II flux suggest that at least part of the Mg II is photoionized by the continuum. This result offers support to use the RM technique to infer the distances of the Mg II broad-line clouds. The associated Mg II variability is reduced compared to the level of continuum changes, which is generally consistent with observations of Mg II variability (Sun et al. 2015) and photoionization calculations (e.g. Goad, O'Brien & Gondhalekar 1993; Guo et al. 2019). The weaker Mg II variability compared with other broad lines (e.g. Hβ) makes it generally more difficult to detect an RM lag for broad Mg II.

On the other hand, for the bulk of EVQs in our sample, the FWHM of broad Mg II does not vary with luminosity as expected from the simple virial assumption, in contrast to the case of broad Hβ. This result suggests that the single-epoch virial BH mass based on Mg II, which depends both on the continuum luminosity and single-epoch Mg II width, will have an additional scatter in individual objects when luminosity varies, while Mg II width remains the same. To demonstrate this point, we estimate single-epoch Mg II-based black hole masses using the bright and faint-state spectra and the recipe from McLure & Dunlop (2004; listed in Table 2). Apart from some quasars with small continuum changes (since some EVQs brightened again in our late GMOS spectroscopy) and some quasars with bad spectral quality, the black hole mass estimates in the bright and faint states are inconsistent (at $>1\sigma$ of measurement errors) for eight of the EVQs in our main sample, including J2159+0005, J2252+0004, J2249+0047, J2228−0032, J2328−0053, J2335−0049, J2141−0016, and J2209−0055. For example, the black hole mass estimates for J2159+0005 are $(1.48 \pm 0.17) \times 10^9$ $M_\odot$ in the bright state and $(5.03 \pm 1.18) \times 10^8$ $M_\odot$ in the dim state. These two black hole masses are inconsistent at $>4\sigma$ confidence level. Using the width of broad Mg II to estimate the black hole mass therefore introduces a luminosity-dependent bias (see detailed discussion in Shen 2013) with the single-epoch mass technique that is most severe for quasars that undergo significant luminosity changes. For individual quasars, clearly the $R - L$ relation is different or even absent for broad Mg II, although there may still be a global $R - L$ relation for quasars over a broad range of luminosity. The latter case will justify the use of Mg II as an single-epoch mass estimator for the general population of quasars (albeit still suffering from the luminosity-dependent scatter in individual objects), and the existence of such a global $R - L$ relation for broad Mg II can be tested with upcoming RM results on large quasar samples (e.g. Shen et al. 2015; Czerny et al. 2019; Grier et al. 2019; Hoormann et al. 2019; Shen et al. 2019).

As luminosity increases, clouds at larger radii in the BLR will fulfil the ionization requirements to produce line emission, and thus the observed (flux-weighted) line width decreases. This phenomenon, the so-called breathing effect, is observed conclusively for Hβ (Korista & Goad 2004; Cackett & Horne 2006; Denney et al. 2009;

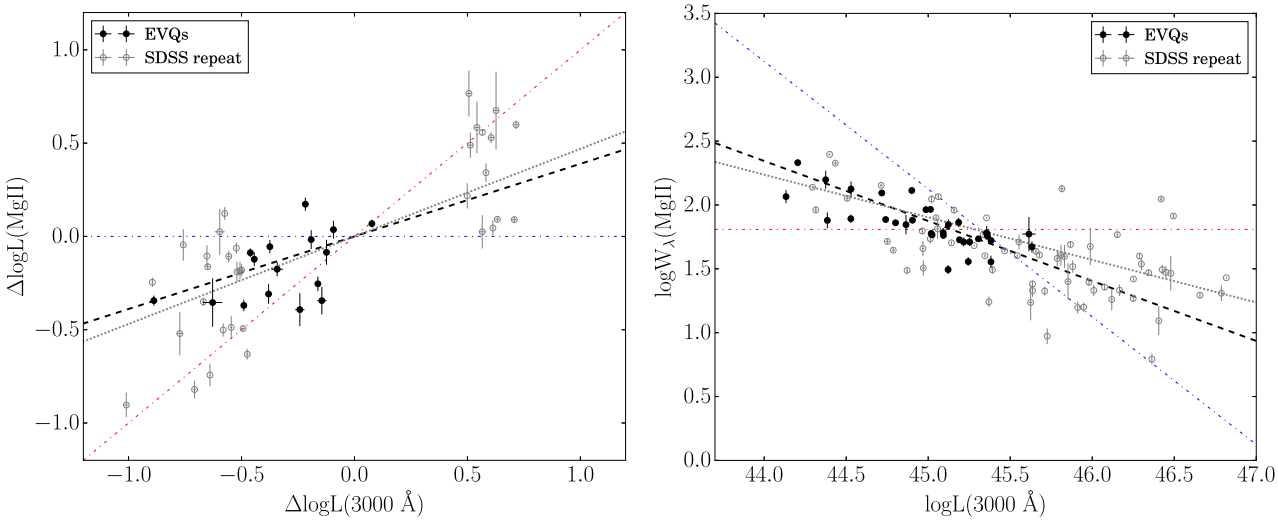

Figure 3. Left: the broad Mg II luminosity variability as a function of the continuum luminosity variability between two epochs of spectroscopy. Both the line and continuum variability measures the changes from the earlier epoch to the later epoch. The filled black dots are the 16 EVQs selected from SDSS+DES imaging and followed up with GMOS spectroscopy, and the open grey circles represent the supplemental EVQs selected from SDSS spectroscopy alone. The Mg II broad line luminosity increases when the continuum luminosity increases, but with a slope shallower than 1. Right: the relation between the equivalent width of broad Mg II and the continuum luminosity. In both panels, the red dot–dashed line shows the one-to-one relation between the (fractional) variability of the line and the continuum, and the blue dot–dashed line corresponds to constant line flux independent of continuum changes. These two cases are the two extreme cases where the Mg II line either fully responds to the continuum changes or does not respond at all. On average these quasars are between these two extreme cases. The black dashed line and grey dotted line are the best-fitting linear regression results for the main sample and the combined sample.

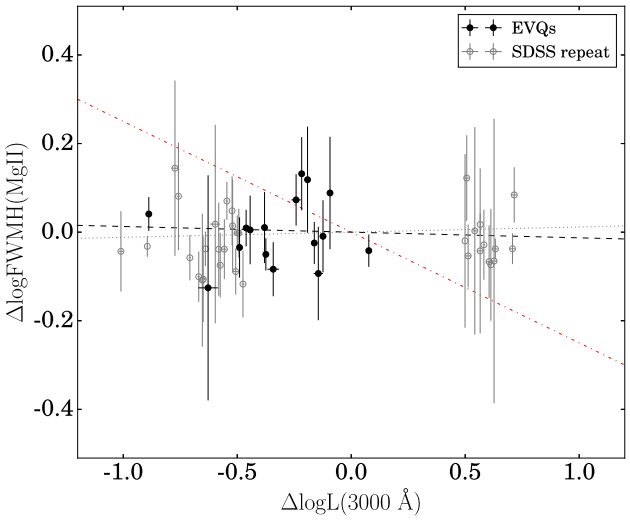

Figure 4. Broad Mg II FWHM variability versus continuum variability. The red dotted line indicates the expected virial relation of $\Delta \log W = -0.25 \Delta \log L$. The FWHM of broad Mg II does not vary accordingly in response to changes in the continuum (see Section 4.2 for details).

Park et al. 2012; Barth et al. 2015; Runco et al. 2016). Different from Hβ as a recombination line, Mg II are mainly collisionally excited. The greater optical depth for Mg II, which results in a large number of scatterings before escape from the BLR, may cause the Mg II photons to be emitted over a larger radius than Hβ (Korista & Goad 2004). Thus the variation in ionizing continuum may be diluted at a larger radius, leading to a smaller amplitude of Mg II variability. The lack of a clear intrinsic $R - L$ relation for broad Mg II could mean that the broad Mg II emission is mostly confined in a narrower range of radii than the broader distribution of gas that can potentially produce Hβ emission. The transition layer between the H II zone and the H I zone, where most of the continuum photons between 13.6 and 55 eV are absorbed and a large portion of the line emission is produced, is geometrically thin (Krolik 1999). This layer could emit a larger fraction of the total Mg II emission than it does for the total Balmer-line emission (e.g. Kwan & Krolik 1981). Thus when the ionizing continuum changes, the flux of Mg II echoes, but the average radius of the gas emitting Mg II barely changes, leading to more or less constant broad Mg II width. Detailed photoionization calculations seem to support this scenario (e.g. Goad et al. 1993; Korista & Goad 2004; Guo et al. 2019). Another possibility is that part of gas emitting Mg II is virialized and photoionized, while the other part is not. It has been shown that Mg II profile is complex (Kovačević-Dojčinović & Popović 2015; Jonić et al. 2016), and can be affected by non-virial effects, such as outflows (León-Tavares et al. 2013; Popović, Kovačević-Dojčinović & Marčeta-Mandić 2019), especially for very broad Mg II (FWHM $> 6000\,\mathrm{km\,s^{-1}}$). Potential detailed shape change of Mg II profile can be analysed with dedicated Mg II RM data and used to test these scenarios.

There are some cases where the extreme variability of quasars can be reasonably well explained by microlensing (e.g. Lawrence et al. 2016; Bruce et al. 2017), with a smooth, bell-shaped light curve. The light curve of J2159+0005 is smooth, but cannot be well fitted by a simple point source, point-lens microlensing model. As described in Lawrence et al. (2016) and Bruce et al. (2017), microlensing events cannot explain all hypervariable AGN activity, but likely explain a sub-set of them. It is possible that some of these large-amplitude variations are due to microlensing that can be fitted by more complicated lensing models.

6 SUMMARY

We have presented Gemini/GMOS spectroscopy of 16 EVQs, with >1.5 mag maximum variability in the g band from the combined DES and SDSS photometric light curves (Rumbaugh

et al. 2018), and studied their spectral changes between the GMOS spectra and the earlier SDSS spectra.

Our main results are:

(1) About half of the EVQs brightened again a few years since reaching the minimum flux. This is consistent with the conclusions in Rumbaugh et al. (2018) that extreme variability events are common among the general population of quasars on multiyear time-scales, as well as the findings in the recent spectroscopic work by MacLeod et al. (2019). The extreme variability can also occur, albeit much less frequently, on much shorter time-scales of <1 yr, consistent with the findings in previous studies (Gezari et al. 2017; Yang et al. 2018; Trakhtenbrot et al. 2019).

(2) We identified two quasars that apparently changed their spectroscopic appearance. J2159+0005 is a possible CLQ. If confirmed, it would be the most distant CLQ so far discovered at $z = 0.936$. J2343+0038 is a CLQ, at $z = 0.667$, based on the disappearance of Hβ.

(3) The Mg II broad line flux varies accordingly as the continuum changes, albeit with a smaller amplitude than that for the continuum, $\Delta\log L(\mathrm{Mg\,II}) = (0.39 \pm 0.07) \times \Delta\log L(3000\,\text{Å})$. This suggests that at least part of the broad Mg II emission is photoionized, or the continuum flux that ionizes broad Mg II varies less than the continuum at rest-frame 3000 Å.

(4) The Mg II broad line FWHM remains roughly constant for the bulk of the objects, even though the continuum luminosity changed significantly, in contrast to the properties of broad Hβ. We discussed potential causes of the different kinematic properties of the broad Mg II line, but to confirm these speculations require future dedicated Mg II RM data. Nevertheless, the different variability properties of broad Mg II compared to broad Hβ provide some cautionary notes on the use of Mg II as a single-epoch BH mass estimator. In particular, the absence of a clear intrinsic $R - L$ relation for Mg II will inevitably lead to a luminosity-dependent bias in the BH mass estimates in individual systems as the continuum luminosity varies significantly.

ACKNOWLEDGEMENTS

We thank the referee, Andy Lawrence, for useful comments that improved the manuscript. QY and YS acknowledge support from an Alfred P. Sloan Research Fellowship (YS) and NSF grant AST-1715579. We thank Patrick Hall, Tamara Davis, Shu Wang, and Hengxiao Guo for useful discussions and suggestions.

Funding for the DES Projects has been provided by the U.S. Department of Energy, the U.S. National Science Foundation, the Ministry of Science and Education of Spain, the Science and Technology Facilities Council of the United Kingdom, the Higher Education Funding Council for England, the National Center for Supercomputing Applications at the University of Illinois at Urbana-Champaign, the Kavli Institute of Cosmological Physics at the University of Chicago, the Center for Cosmology and Astro-Particle Physics at the Ohio State University, the Mitchell Institute for Fundamental Physics and Astronomy at Texas A&M University, Financiadora de Estudos e Projetos, Fundação Carlos Chagas Filho de Amparo à Pesquisa do Estado do Rio de Janeiro, Conselho Nacional de Desenvolvimento Científico e Tecnológico and the Ministério da Ciência, Tecnologia e Inovação, the Deutsche Forschungsgemeinschaft, and the Collaborating Institutions in the Dark Energy Survey.

The Collaborating Institutions are Argonne National Laboratory, the University of California at Santa Cruz, the University of Cambridge, Centro de Investigaciones Energéticas, Medioambientales y Tecnológicas-Madrid, the University of Chicago, University College London, the DES-Brazil Consortium, the University of Edinburgh, the Eidgenössische Technische Hochschule (ETH) Zürich, Fermi National Accelerator Laboratory, the University of Illinois at Urbana-Champaign, the Institut de Ciències de l'Espai (IEEC/CSIC), the Institut de Física d'Altes Energies, Lawrence Berkeley National Laboratory, the Ludwig-Maximilians Universität München and the associated Excellence Cluster Universe, the University of Michigan, the National Optical Astronomy Observatory, the University of Nottingham, The Ohio State University, the University of Pennsylvania, the University of Portsmouth, SLAC National Accelerator Laboratory, Stanford University, the University of Sussex, Texas A&M University, and the OzDES Membership Consortium.

Based in part on observations at Cerro Tololo Inter-American Observatory, National Optical Astronomy Observatory, which is operated by the Association of Universities for Research in Astronomy (AURA) under a cooperative agreement with the National Science Foundation.

The DES data management system is supported by the National Science Foundation under Grant Numbers AST-1138766 and AST-1536171. The DES participants from Spanish institutions are partially supported by MINECO under grants AYA2015-71825, ESP2015-66861, FPA2015-68048, SEV-2016-0588, SEV-2016-0597, and MDM-2015-0509, some of which include ERDF funds from the European Union. IFAE is partially funded by the CERCA program of the Generalitat de Catalunya. Research leading to these results has received funding from the European Research Council under the European Union's Seventh Framework Program (FP7/2007-2013) including ERC grant agreements 240672, 291329, and 306478. We acknowledge support from the Brazilian Instituto Nacional de Ciênciae Tecnologia (INCT) e-Universe (CNPq grant 465376/2014-2).

This manuscript has been authored by Fermi Research Alliance, LLC under Contract No. DE-AC02-07CH11359 with the U.S. Department of Energy, Office of Science, Office of High Energy Physics. The United States Government retains and the publisher, by accepting the article for publication, acknowledges that the United States Government retains a non-exclusive, paid-up, irrevocable, world-wide license to publish or reproduce the published form of this manuscript, or allow others to do so, for United States Government purposes.

Funding for SDSS-III has been provided by the Alfred P. Sloan Foundation, the Participating Institutions, the National Science Foundation, and the U.S. Department of Energy Office of Science. The SDSS-III website is http://www.sdss3.org/. SDSS-III is managed by the Astrophysical Research Consortium for the Participating Institutions of the SDSS-III Collaboration including the University of Arizona, the Brazilian Participation Group, Brookhaven National Laboratory, Carnegie Mellon University, University of Florida, the French Participation Group, the German Participation Group, Harvard University, the Instituto de Astrofisica de Canarias, the Michigan State/Notre Dame/JINA Participation Group, Johns Hopkins University, Lawrence Berkeley National Laboratory, Max Planck Institute for Astrophysics, Max Planck Institute for Extraterrestrial Physics, New Mexico State University, New York University, Ohio State University, Pennsylvania State University, University of Portsmouth, Princeton University, the Spanish Participation Group, University of Tokyo, University of Utah, Vanderbilt University, University of Virginia, University of Washington, and Yale University.

The PS1 has been made possible through contributions by the 'Institute for Astronomy', the University of Hawaii, the 'Pan-STARRS Project Office', the 'Max-Planck Society' and its participating institutes, the 'Max Planck Institute for Astronomy, Heidelberg', and the 'Max Planck Institute for Extraterrestrial Physics, Garching', 'The Johns Hopkins University', Durham University, the University of Edinburgh, 'Queen's University Belfast', the Harvard-Smithsonian Center for Astrophysics, the 'Las Cumbres Observatory Global Telescope Network Incorporated', 'the National Central University of Taiwan', the Space Telescope Science Institute, the National Aeronautics and Space Administration under Grant No. NNX08AR22G issued through the Planetary Science Division of the NASA Science Mission Directorate, the National Science Foundation under Grant No. AST-1238877, the University of Maryland, and Eotvos Lorand University (ELTE).

REFERENCES

Abazajian K. N. et al., 2009, ApJS, 182, 543
Abbott T. M. C. et al., 2018, ApJS, 239, 18
Antonucci R., 1993, ARA&A, 31, 473
Baldwin J. A., 1977, ApJ, 214, 679
Barth A. J. et al., 2015, ApJS, 217, 26
Boroson T. A., Green R. F., 1992, ApJS, 80, 109
Bruce A. et al., 2017, MNRAS, 467, 1259
Cackett E. M., Horne K., 2006, MNRAS, 365, 1180
Cackett E. M., Gültekin K., Bentz M. C., Fausnaugh M. M., Peterson B. M., Troyer J., Vestergaard M., 2015, ApJ, 810, 86
Cardelli J. A., Clayton G. C., Mathis J. S., 1989, ApJ, 345, 245
Chambers K. C. et al., 2016, preprint (arXiv:1612.05560)
Clavel J. et al., 1991, ApJ, 366, 64
Czerny B. et al., 2019, ApJ, 880, 46
Denney K. D., Peterson B. M., Dietrich M., Vestergaard M., Bentz M. C., 2009, ApJ, 692, 246
Denney K. D. et al., 2014, ApJ, 796, 134
Diehl H. T. et al., 2018, Proc. SPIE Conf. Ser. Vol. 10704, Observatory Operations: Strategies, Processes, and Systems VII. SPIE, Bellingham, p. 107040D
Flaugher B. et al., 2015, AJ, 150, 150
Frieman J. A. et al., 2008, AJ, 135, 338
Gezari S. et al., 2017, ApJ, 835, 144
Goad M. R., O'Brien P. T., Gondhalekar P. M., 1993, MNRAS, 263, 149
Green P. J., Forster K., Kuraszkiewicz J., 2001, ApJ, 556, 727
Grier C. J. et al., 2019, ApJ, 887, 38
Gunn J. E. et al., 2006, AJ, 131, 2332
Guo H., Gu M., 2016, ApJ, 822, 26
Guo H. et al., 2019, ApJ, 887, 58
Hoormann J. K. et al., 2019, MNRAS, 487, 3650
Hryniewicz K., Czerny B., Pych W., Udalski A., Krupa M., Świętoń A., Kaluzny J., 2014, A&A, 562, A34
Ivezić Ž. et al., 2007, AJ, 134, 973
Jonić S., Kovačević-Dojčinović J., Ilić D., Popović L. Č., 2016, Ap&SS, 361, 101
Korista K. T., Goad M. R., 2004, ApJ, 606, 749
Kovačević-Dojčinović J., Popović L. Č., 2015, ApJS, 221, 35
Krolik J. H., 1999, Active galactic nuclei : from the central black hole to the galactic environment. Princeton Univ. Press, Princeton
Kwan J., Krolik J. H., 1981, ApJ, 250, 478
LaMassa S. M. et al., 2015, ApJ, 800, 144
Lawrence A., 2018, Nature Astron., 2, 102
Lawrence A. et al., 2016, MNRAS, 463, 296
León-Tavares J. et al., 2013, ApJ, 763, L36
MacLeod C. L. et al., 2012, ApJ, 753, 106
MacLeod C. L. et al., 2016, MNRAS, 457, 389
MacLeod C. L. et al., 2019, ApJ, 874, 8
McElroy R. E. et al., 2016, A&A, 593, L8
McLure R. J., Dunlop J. S., 2004, MNRAS, 352, 1390
McLure R. J., Jarvis M. J., 2002, MNRAS, 337, 109
Metzroth K. G., Onken C. A., Peterson B. M., 2006, ApJ, 647, 901
Morganson E. et al., 2014, ApJ, 784, 92
Pâris I. et al., 2018, A&A, 613, A51
Park D. et al., 2012, ApJ, 747, 30
Popović L. Č., Kovačević-Dojčinović J., Marčeta-Mandić S., 2019, MNRAS, 484, 3180
Reichert G. A. et al., 1994, ApJ, 425, 582
Roig B., Blanton M. R., Ross N. P., 2014, ApJ, 781, 72
Ross N. P. et al., 2018, MNRAS, 480, 4468
Ruan J. J. et al., 2016, ApJ, 826, 188
Rumbaugh N. et al., 2018, ApJ, 854, 160
Runco J. N. et al., 2016, ApJ, 821, 33
Runnoe J. C. et al., 2016, MNRAS, 455, 1691
Salviander S., Shields G. A., Gebhardt K., Bonning E. W., 2007, ApJ, 662, 131
Schlegel D. J., Finkbeiner D. P., Davis M., 1998, ApJ, 500, 525
Schmidt K. B., Marshall P. J., Rix H.-W., Jester S., Hennawi J. F., Dobler G., 2010, ApJ, 714, 1194
Sesar B. et al., 2007, AJ, 134, 2236
Shen Y., 2013, Bull. Astron. Soc. India, 41, 61
Shen Y., Greene J. E., Strauss M. A., Richards G. T., Schneider D. P., 2008, ApJ, 680, 169
Shen Y. et al., 2011, ApJS, 194, 45
Shen Y. et al., 2015, ApJS, 216, 4
Shen Y. et al., 2016, ApJ, 818, 30
Shen Y. et al., 2019, ApJ, 241, 34
Shen Y. et al., 2019, ApJ, 883, L14
Stern D. et al., 2018, ApJ, 864, 27
Sun M. et al., 2015, ApJ, 811, 42
Tody D., 1986, in Crawford D. L., ed., Proc. SPIE Conf. Ser. Vol. 627, Instrumentation in astronomy VI. SPIE, Belingham, p. 733
Tody D., 1993, in Hanisch R. J., Brissenden R. J. V., Barnes J., eds, ASP Conf. Ser. Vol. 52, Astronomical Data Analysis Software and Systems II. Astron. Soc. Pac., San Francisco, p. 173
Trakhtenbrot B. et al., 2019, ApJ, 883, 94
Trevese D., Paris D., Stirpe G. M., Vagnetti F., Zitelli V., 2007, A&A, 470, 491
Tsuzuki Y., Kawara K., Yoshii Y., Oyabu S., Tanabé T., Matsuoka Y., 2006, ApJ, 650, 57
Urry C. M., Padovani P., 1995, PASP, 107, 803
Vanden Berk D. E. et al., 2004, ApJ, 601, 692
Vestergaard M., Wilkes B. J., 2001, ApJS, 134, 1
Wandel A., Peterson B. M., Malkan M. A., 1999, ApJ, 526, 579
Wang S. et al., 2019, ApJ, 882, 4
Wang J.-G. et al., 2009, ApJ, 707, 1334
Wilhite B. C., Vanden Berk D. E., Kron R. G., Schneider D. P., Pereyra N., Brunner R. J., Richards G. T., Brinkmann J. V., 2005, ApJ, 633, 638
Woo J.-H., 2008, AJ, 135, 1849
Yang Q. et al., 2018, ApJ, 862, 109
Zhu D., Sun M., Wang T., 2017, ApJ, 843, 30

APPENDIX A:

The light curves and spectra of the remaining 14 EVQs, in addition to the two shown in Fig. 1, are provided in Fig. A1, in the same order as that in Table 1 in terms of the level of dimming.

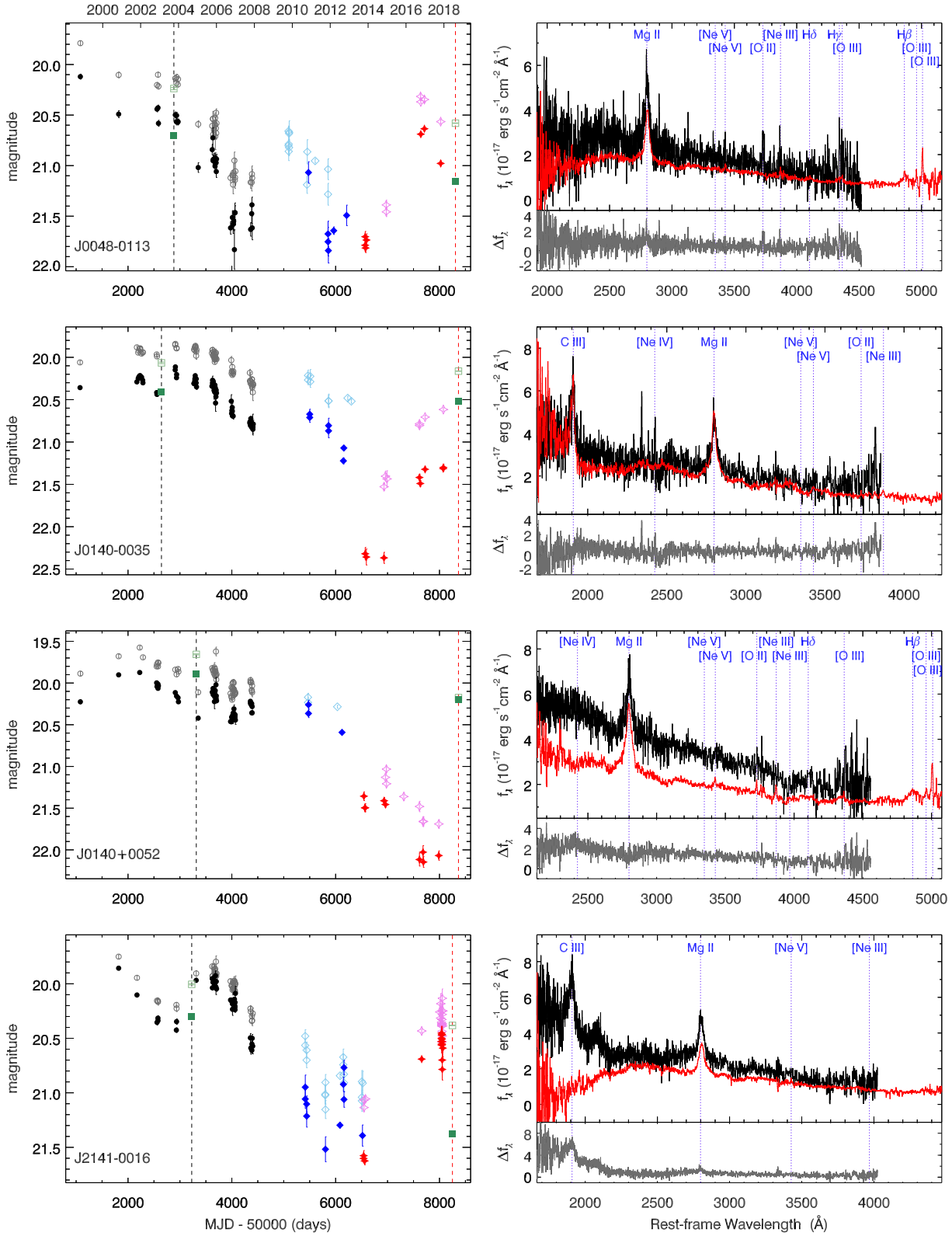

Figure A1. The rest of the EVQ sample observed with GMOS. Notations are the same as Fig. 1.

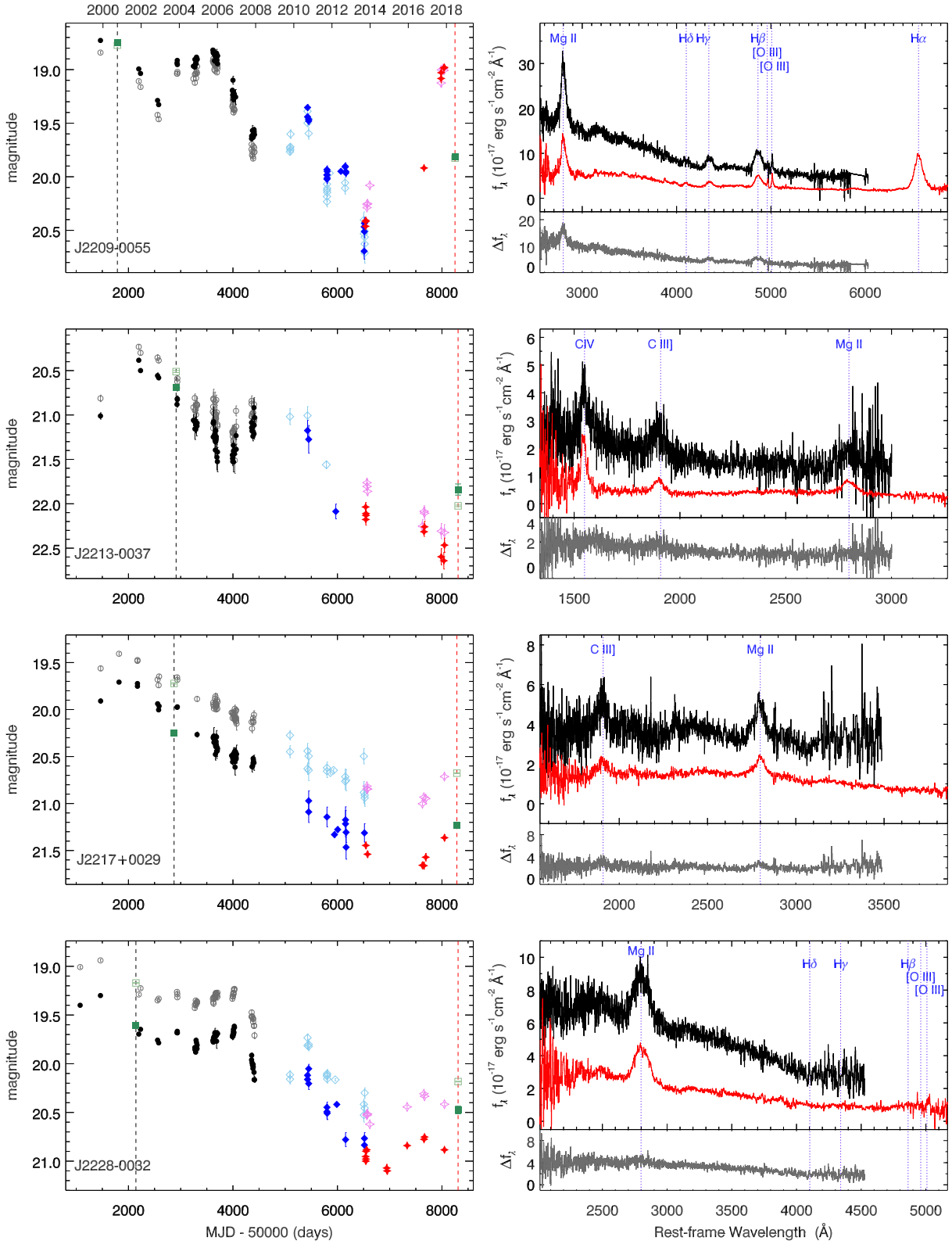

Figure A1. (Continued.)

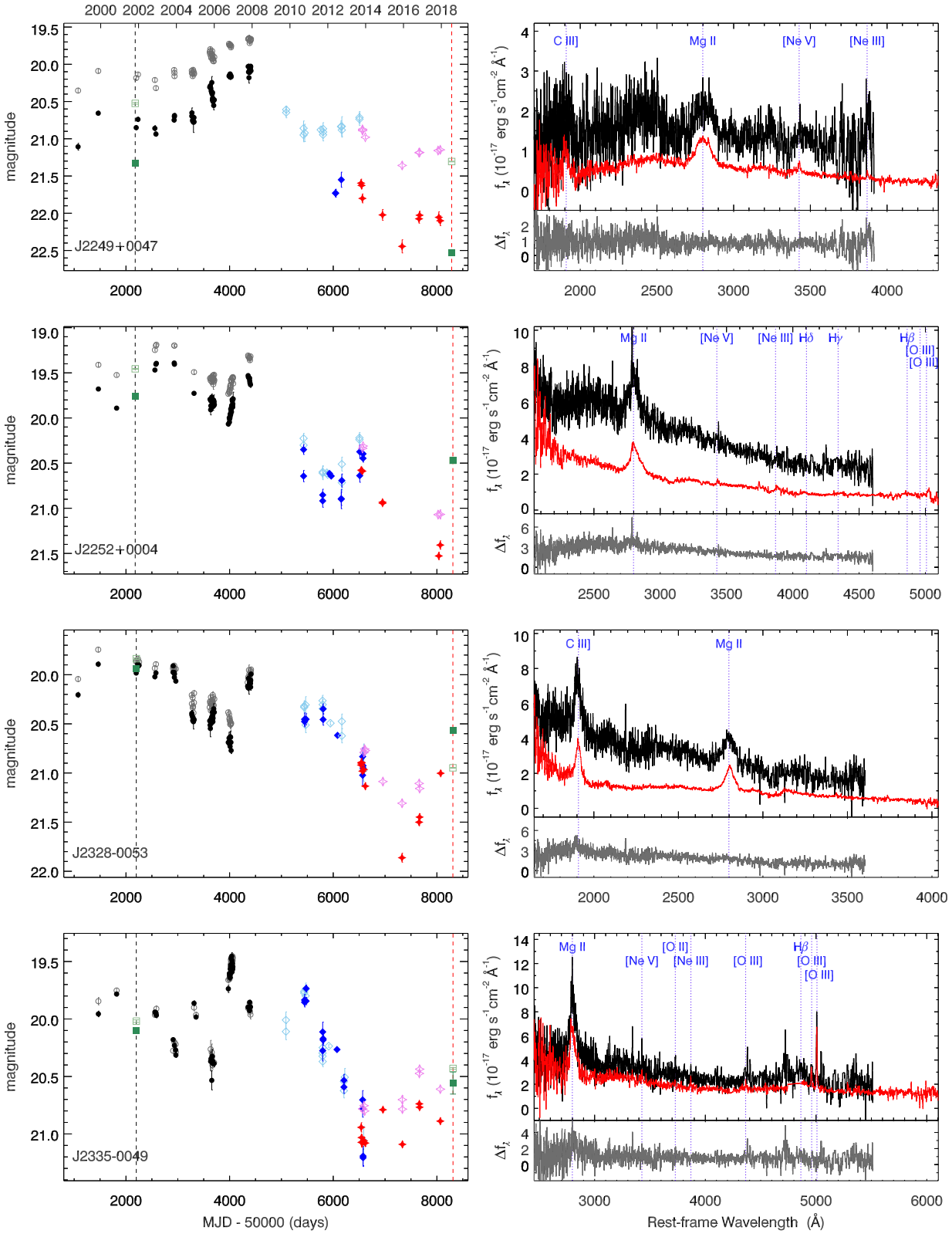

Figure A1. (Continued.)

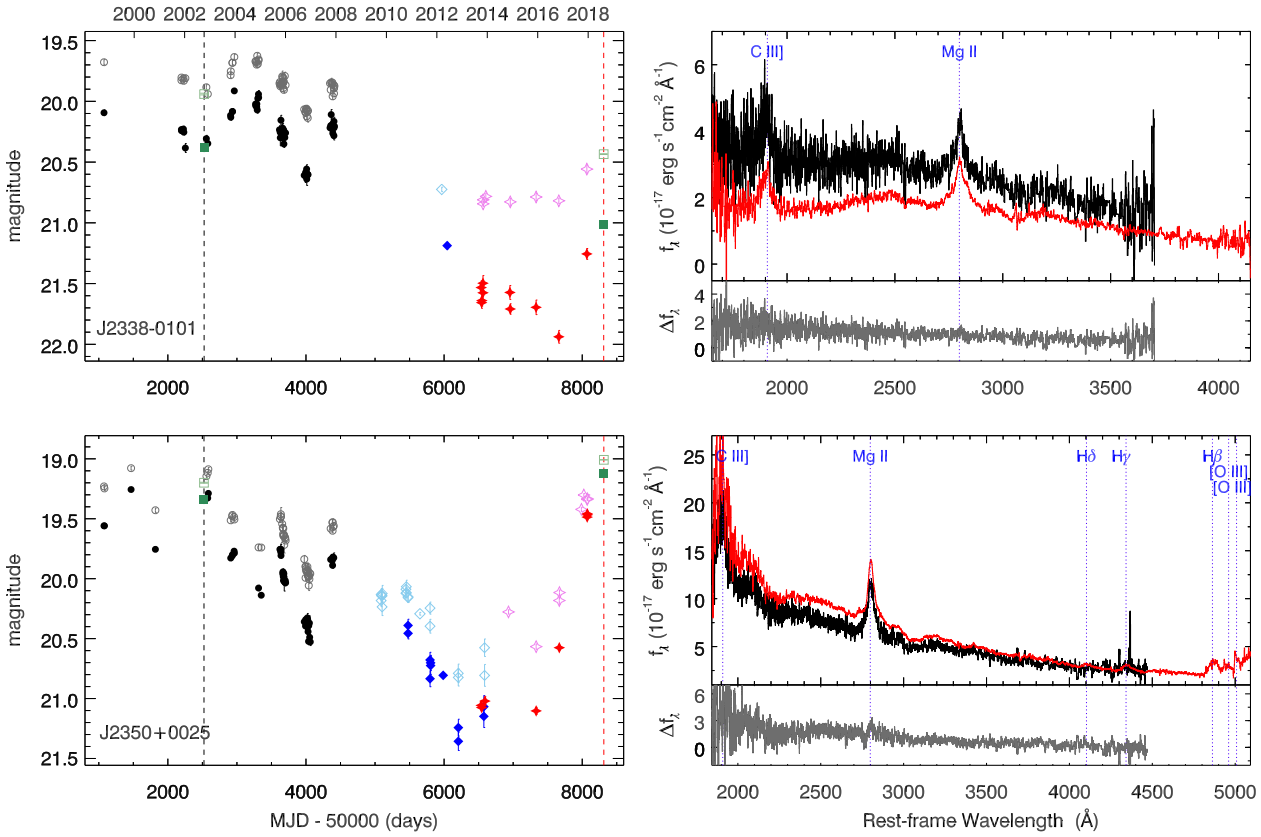

Figure A1. (Continued.)

[1]*Department of Astronomy, University of Illinois at Urbana-Champaign, Urbana, IL 61801, USA*
[2]*National Center for Supercomputing Applications, University of Illinois at Urbana-Champaign, Urbana, IL 61801, USA*
[3]*Fermi National Accelerator Laboratory, PO Box 500, Batavia, IL 60510, USA*
[4]*Instituto de Fisica Teorica UAM/CSIC, Universidad Autonoma de Madrid, E-28049 Madrid, Spain*
[5]*CNRS, Institut d'Astrophysique de Paris, UMR 7095, F-75014, Paris, France*
[6]*Institut d'Astrophysique de Paris, Sorbonne Universités, UPMC Univ Paris 06, UMR 7095, F-75014, Paris, France*
[7]*Department of Physics & Astronomy, University College London, Gower Street, London, WC1E 6BT, UK*
[8]*Laboratório Interinstitucional de e-Astronomia - LIneA, Rua Gal. José Cristino 77, Rio de Janeiro, RJ - 20921-400, Brazil*
[9]*Centro de Investigaciones Energéticas, Medioambientales y Tecnológicas (CIEMAT), 28040 Madrid, Spain*
[10]*Institut de Física d'Altes Energies (IFAE), The Barcelona Institute of Science and Technology, Campus UAB, E-08193 Bellaterra, Spain*
[11]*Observatório Nacional, Rua Gal. José Cristino 77, Rio de Janeiro, RJ - 20921-400, Brazil*
[12]*Department of Physics, IIT Hyderabad, Kandi, Telangana 502285, India*
[13]*Kavli Institute for Cosmological Physics, University of Chicago, Chicago, IL 60637, USA*
[14]*Institut d'Estudis Espacials de Catalunya (IEEC), 08193 Barcelona, Spain*
[15]*Institute of Space Sciences (ICE, CSIC), Campus UAB, Carrer de Can Magrans, s/n, E008193 Barcelona, Spain*
[16]*Department of Astronomy, University of Michigan, Ann Arbor, MI 48109, USA*
[17]*Department of Physics, University of Michigan, Ann Arbor, MI 48109, USA*
[18]*SLAC National Accelerator Laboratory, Menlo Park, CA 94025, USA*
[19]*Kavli Institute for Particle Astrophysics & Cosmology, Stanford University, PO Box 2450, Stanford, CA 94305, USA*
[20]*Santa Cruz Institute for Particle Physics, Santa Cruz, CA 95064, USA*
[21]*Department of Physics, The Ohio State University, Columbus, OH 43210, USA*
[22]*Center for Cosmology and Astro-Particle Physics, The Ohio State University, Columbus, OH 43210, USA*
[23]*Max Planck Institute for Extraterrestrial Physics, Giessenbachstrasse, D-85748 Garching, Germany*
[24]*Fakultät für Physik, Ludwig-Maximilians Universität MünchenUniversitäts-Sternwarte, Scheinerstr. 1, D-81679 München, Germany*
[25]*Harvard-Smithsonian Center for Astrophysics, Cambridge, MA 02138, USA*
[26]*Department of Astronomy/Steward Observatory, 933 North Cherry Avenue, Tucson, AZ 85721-0065, USA*
[27]*Australian Astronomical Observatory, North Ryde, NSW 2113, Australia*
[28]*The Research School of Astronomy and Astrophysics, Australian National University, ACT 2601, Australia*
[29]*Departamento de Física Matemática, Instituto de Física, Universidade de São Paulo, CP 66318, São Paulo, SP, 05314-970, Brazil*
[30]*George P. and Cynthia Woods Mitchell Institute for Fundamental Physics and Astronomy, and Department of Physics and Astronomy, Texas A&M University, College Station, TX 77843, USA*
[31]*Department of Astronomy, The Ohio State University, Columbus, OH 43210, USA*

[32]*Institució Catalana de Recerca i Estudis Avançats, E-08010 Barcelona, Spain*
[33]*Department of Astrophysical Sciences, Princeton University, Peyton Hall, Princeton, NJ 08544, US*
[34]*School of Physics and Astronomy, University of Southampton, Southampton, SO17 1BJ, UK*
[35]*Department of Physics, Brandeis University, Waltham, MA 02453, USA*
[36]*Instituto de Física Gleb Wataghin, Universidade Estadual de Campinas, 13083-859 Campinas, SP, Brazil*
[37]*Computer Science and Mathematics Division, Oak Ridge National Laboratory, US, Oak Ridge, TN 37831*
[38]*Argonne National Laboratory, 9700 South Cass Avenue, Lemont, IL 60439, USA*
[39]*Cerro Tololo Inter-American Observatory, National Optical Astronomy Observatory, Casilla 603, La Serena, Chile*

This paper has been typeset from a TEX/LATEX file prepared by the author.